JCTC Journal of Chemical Theory and Computation

Article

pubs.acs.org/JCTC

Solvation Station: Microsolvation for Modeling Vibrational Sum-Frequency Spectra of Acids at Aqueous Interfaces

Nicholas A. Valley and Geraldine L. Richmond*

Department of Chemistry, University of Oregon, Eugene, Oregon 97403, United States

Supporting Information

ABSTRACT: Vibrational sum-frequency spectra of a pair of poly(methacrylic acid) isomers at an oil/water interface and glutaric acid at an air/water interface were calculated in the carbonyl stretching region. Orientational, conformational, and solvation information was determined using classical molecular dynamics (MD), while second-order susceptibility vibrational response tensors were determined for a set of density functional theory (DFT) structures. The DFT structures were microsolvated with water molecules corresponding to the major solvation states present in the MD calculations. The inclusion of the microsolvating waters incorporates solvation effects important to the carboxylic acid stretching modes in the studied spectral region. The calculated spectra strongly agree with experimental spectra when a cutoff of 1.975 Å is used to define a hydrogen bond in the MD trajectories. With the chosen cutoff, the most common solvation state of the carboxylic acid moieties involves a single hydrogen bond to the carbonyl oxygen and a single hydrogen bond to the carboxylic acid hydrogen. The sensitivity of the spectra to the hydrogen bond cutoff definition and the included DFT structures was investigated. Moderate changes in the relative intensities of the contributing peaks were found in both cases. Shortening the hydrogen bond cutoff definition predictably leads to a decrease in the relative intensity of peaks corresponding to well-solvated structures, while altering the set of DFT solvation structures results in more complex behavior that is dependent on the specific structures included.

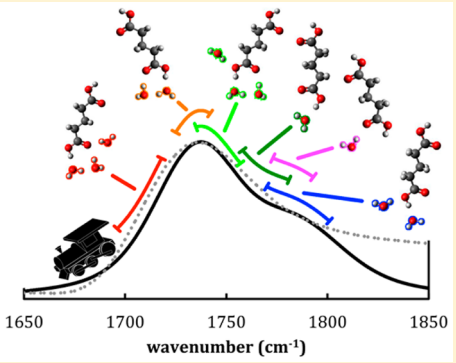

1. INTRODUCTION

Vibrational sum-frequency (VSF) spectroscopy is a powerful tool for understanding the interfacial behavior and alignment of molecules. Applications of VSF spectroscopy have provided pertinent information for understanding interfacial processes important to atmospheric chemistry, environmental remediation, and industrial applications.[1−15] The complex interferences that occur with VSF generation cause signal to arise only in spatial regions that do not have local inversion symmetry. The advantage of this property is that it results in an interfacially specific technique.[16−18] This very property, however, also leads to difficulty in spectral interpretation because vibrational resonances in close proximity can coherently interfere, altering the experimentally observed peak positions and intensities.

Assigning VSF spectra can therefore prove very difficult, especially in spectral regions with a high density of vibrational states. As interfacial systems of interest become ever more complex, it is increasingly important to be able to confidently calculate VSF spectra to assist in accurate interpretation of experimental spectra and to connect observables to molecular-level behavior. Calculation of VSF spectra presents its own wealth of challenges. Ideally, one requires a complete description of the molecular interfacial orientations as well as the vibrational response of the hyperpolarizability as a function of all of the molecular internal degrees of freedom. The hyperpolarizability is usually approximated as a product of dipole moment (μ) and polarizability (α) derivatives. Such a complete description is too computationally expensive to feasibly calculate VSF spectra for more complex systems of interest. Consequently, various approximations are required.

Efforts looking to generate predictive VSF spectra fall into one of three main categories. All of the methods calculate the frequency-dependent second-order response as a function of conformation and orientation in a dynamical interfacial system; the differences stem from the approximations that make such descriptions feasible. One computational approach uses a dynamical method with at least the molecule of interest being treated quantum-mechanically (ab initio MD,[19] QM/MM[20]). This approach provides an accurate description of the molecular properties in a dynamical system, giving μ and α as well as vibrational frequencies and molecular orientations at the same time. Generally, however, the computational expense restricts the system size to a point where the interface is poorly described and/or the conformational and orientational space of the molecule is not well sampled. Another approach, developed by Morita and Hynes,[21,22] involves a time correlation function analysis of classical molecular dynamics (MD) with analytical forms of the dipole moment and polarizability. It has been used extensively to calculate VSF spectra of water[21−26] and a few

Received: May 22, 2015
Published: August 31, 2015

DOI: 10.1021/acs.jctc.5b00484
J. Chem. Theory Comput. 2015, 11, 4780−4790

other small molecules.[27−30] Using this method for larger molecules proves difficult, as it requires explicit knowledge of how the dipole moment and polarizability transform in regard to the internal molecular geometry, which scales with the cube of the number of atoms.

The approach used here employs classical MD to provide information about interfacial orientations and conformations. A set of gas-phase density functional theory (DFT) structures representative of the conformational space observed in the MD calculations are used to furnish vibrational frequencies and dipole moment and polarizability response properties. This approach has been used to generate accurate VSF spectra for large molecular systems with many internal degrees of freedom.[5,6,14,31,32] However, one of the shortcomings of this approach is that it does not inherently include solvation effects as the other approaches do. The present work builds upon this current implementation to create a straightforward methodology for calculating VSF spectra of large molecular systems that includes a proper description of modes strongly perturbed by solvation.

Effects of solvation are added into the computational description by generating a set of DFT structures that are microsolvated with water molecules. The number and arrangement of water molecules in the DFT structures is made to reflect the solvation states observed in the molecular dynamics trajectories. In this way, effects of solvation on vibrational mode frequencies can be coupled to the molecular interfacial orientation. This work shows that for a relatively small increase in the computational expense that is required to calculate the expanded set of DFT structures, accurate VSF spectra in regions containing strongly solvation-dependent modes can be determined.

To show this, both oil/water and air/water interfacial molecular systems are studied. Experimental VSF spectra and surface tensiometry data for each of the systems are readily available. Molecular dynamics calculations have been previously performed on all of the systems, and in all cases calculated VSF spectra have shown reasonable agreement with experimental measurements in the CH stretching region, providing a confident picture of the surface behavior.[14,31] Qualitative interpretations of interesting spectral features in regions with solvation-dependent modes have been made using experimental spectra, but without calculations that account for solvation, a complete molecular-level description is elusive. The computational methodology presented here additionally allows detailed interpretations of experimental VSF spectra in the carbonyl stretching region.

First, a pair of stereoisomers of poly(methacrylic acid) (PMA) at an oil/water interface is studied. The isotactic isomer (iPMA), with the same configuration at successive polymeric units, and the syndiotactic isomer (sPMA), with alternating configurations at successive polymeric units, have been shown to have marked differences in both their bulk[33−36] and interfacial behavior.[14] The differences in interfacial behavior are borne out in differences in experimental VSF spectra in the carbonyl stretching region, where multiple peaks are observed depending on their degree of solvation. Calculated spectra using gas-phase DFT structures fail to capture this behavior and show only a single peak at the gas-phase frequency. Here, by inclusion of waters in the set of iPMA and sPMA DFT structures, VSF spectra in the carbonyl stretching region are calculated. The strong agreement between the calculated and experimental spectra allows experimental observables to be connected to the orientational picture developed by the classical molecular dynamics calculations. To further support the approach used to calculate solvated VSF spectra, a system involving glutaric acid molecules at an air/water interface is studied. Again, reasonable agreement between the calculated and experimental spectra is achieved using DFT structures with microsolvation, pointing to broader applicability of the methodology. Finally, the dependence of the calculated spectra on computational parameters, namely, the hydrogen bond length cutoff and the selection of DFT structures, is investigated.

2. METHODOLOGY

2.1. Molecular Dynamics Methods. Trajectories of classical MD calculations reported in previous works[14,31] have been reanalyzed in the present work. Full details of the parameters used are available,[14,31] and a brief description is given here. In short, MD calculations were performed using the Amber 12 suite of programs[37] with starting configurations created using the PACKMOL[38] program. The PMA systems contained two polymer chains, each 24 monomer units long, in a 40 Å cube of water adjacent to a 40 Å cube of carbon tetrachloride. The glutaric acid systems contained 16 glutaric acid molecules in a 30 Å cube of water. In both instances, the axis of the box perpendicular to the water interface was extended, and periodic boundary conditions were applied to create a slab system. A 1 fs time step was employed. After minimization and equilibration, data were collected every 100 steps from over 20 ns of evolution at 300 K.

2.2. Quantum-Mechanical Methods. DFT calculations were performed using the B3LYP exchange−correlation functional and the 6-311++G(2d,2p) basis set within the NWChem program package.[39] This level of theory has been shown to provide accurate results for water clusters.[40] Geometry optimization and frequency calculations were performed for conformers of PMA monomers (capped with H atoms with a nuclear mass of 12.01 amu to mimic the bonds to C atoms that exist in the extended polymer chain) and glutaric acid molecules and included up to six water molecules. Water molecules (one per hydrogen bond) were added to the structures to reproduce the number of hydrogen bonds and the atoms involved in hydrogen bonding. Restraints were applied when necessary to retain the desired molecular conformation or number and location of hydrogen bonds. Water molecules were frozen in the frequency calculations by giving their atoms arbitrarily large masses in order to be able to isolate the vibrational response properties of the molecule of interest. Comparison of systems with frozen waters to those without showed minor impact on the calculated vibrational frequencies and atomic displacements. Unscaled harmonic frequencies were used for structures containing microsolvating waters. For structures without microsolvating waters, anharmonic corrections to the vibrational frequencies determined using second-order vibrational perturbation theory within the Gaussian 09 program package[41] were used, providing frequencies in good agreement with gas-phase experiments on similar molecules.[42]

The second-order susceptibility tensor for each structure was constructed using derivatives of the polarizability and dipole moment with respect to the normal coordinates of the vibrational modes:

DOI: 10.1021/acs.jctc.5b00484
J. Chem. Theory Comput. 2015, 11, 4780−4790

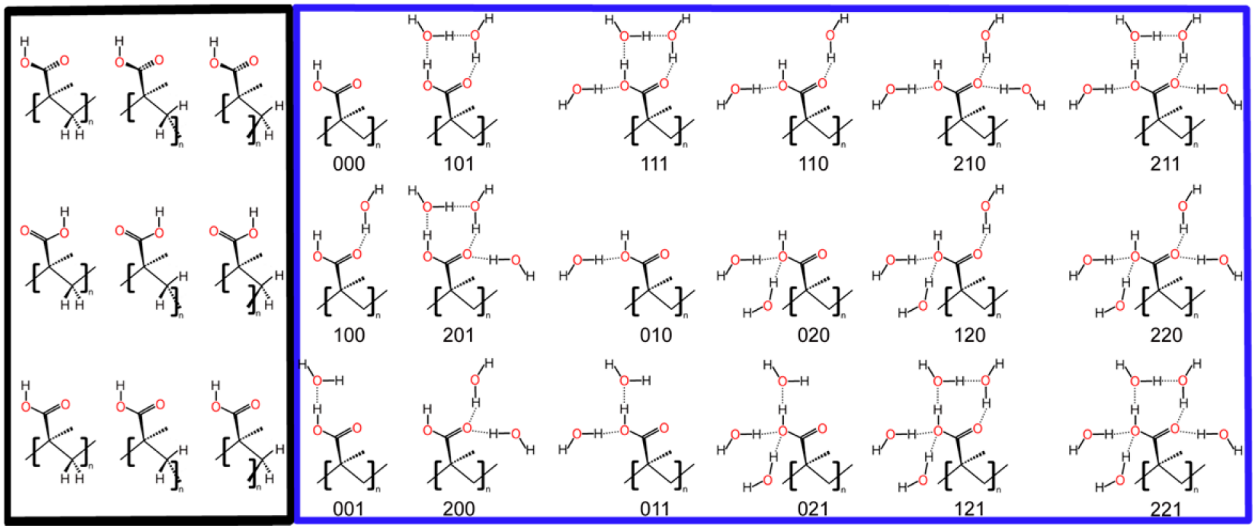

Figure 1. Representations of structures in the conformer set (left black box) and the solvation set (right blue box) of PMA monomers. Solvation set structures include a numeric tag that denotes the number of hydrogen bonds to the carbonyl oxygen, hydroxyl oxygen, and hydroxyl hydrogen.

$$\chi^{(2)}_{ijk,q} \propto \sum_{a,b,c} C_{abc} \frac{\partial \alpha_{ab,q}}{\partial Q_q} \frac{\partial \mu_{c,q}}{\partial Q_q}$$

where α and μ are the molecular polarizability and dipole moment, respectively, Q_q is the normal coordinate of mode q, and C is a geometrical factor that relates the molecular and laboratory reference frames.

2.3. VSF Calculation Methodology. VSF spectra are calculated following a protocol that seeks to balance accurate prediction of experimental spectra with practical concerns of computational expense. MD trajectories are analyzed to procure information pertaining to the molecular conformations and solvation state of each molecule of interest, including internal molecular dihedral angles and hydrogen bond distances between the appropriate atoms in the molecules of interest and water.

On the basis of the dihedral angles and numbers of hydrogen bonds at specific sites, each structure in the MD trajectory is matched to a single microsolvated DFT structure from a set of DFT structures. The set is generated to cover a large portion of the conformational and hydrogen-bonding space spanned in the MD calculations. The chosen DFT structure is rotated to closely match the molecular orientation (relative to the interface) of the corresponding MD structure. The equivalent transformation is used to rotate the dipole moment and polarizability derivative tensors into the laboratory (MD) reference frame.

This procedure is repeated for each MD structure at each time step and used to calculate the second-order susceptibility tensor for the interfacial system. Spectral intensities are proportional to the absolute squares of specific tensor elements determined by the experimental polarization setup. The spectra presented here were calculated using the χ_{xxz} tensor element and thus are comparable to experimental spectra collected with an SSP polarization scheme,[43] where the three letters denote the polarizations of the sum-frequency, visible, and IR beams relative to the plane of incidence (S = perpendicular; P = parallel). The calculated spectra were broadened using a convolution of Lorentzian and Gaussian functions. The Lorentzian line width was 5 cm^{-1}, which is the same as that used for fitting of experimental carbonyl stretching modes based on vibrational relaxation lifetimes.[14,31,44] The Gaussian line width was fixed at 40 cm^{-1} for all modes, which is comparable to values obtained in the experimental fits.[14,31]

3. RESULTS AND DISCUSSION

3.1. Poly(methacrylic acid) Solvation Structures. Simulation of VSF spectra is achieved by combining information from molecular dynamics simulations and gas-phase density functional theory calculations. This approach has been shown to accurately calculate VSF spectra in regions with vibrational modes that are not substantially affected by solvation.[5,14,31,32] To be able to calculate spectra in regions where water solvation is strongly impactful, microsolvating waters have been added to the density functional theory calculations to generate an expanded set of structures that take into account different degrees of solvation. This approach is validated here by two groups of systems: first, an oil/water interface with isotactic (iPMA) and syndiotactic (sPMA) stereoisomers of poly(methacrylic acid), and second, an air/water interface with glutaric acid.

The iPMA and sPMA stereoisomers show contrasting oil/water interfacial behavior. One way that this is manifested is by differences in the carbonyl stretching region of the experimental VSF spectra. The experimental spectra of both iPMA and sPMA reveal a pair of features, a dominant peak at ~1730 cm^{-1} and a strong shoulder at ~1770 cm^{-1}, that correspond to carbonyl stretches in the carboxylic acid moiety. The relative intensity of the shoulder is greater for iPMA than for sPMA. The two features in the experimental spectra can be interpreted as corresponding to carbonyls with stronger and weaker degrees of solvation, respectively, indicating that stronger solvation occurs with sPMA. Previous studies indicated that the difference in solvation arises from differences in the overall arrangement of the polymers at the interface. The experimental data, however, can provide neither the exact corresponding structures nor their relative populations. Using previous methodology that considers only gas-phase DFT structures cannot resolve this issue, as it leads to calculated VSF spectra for both iPMA and sPMA with a single feature that appears at ~1770 cm^{-1}. Carbonyl modes are well-known to be strongly influenced by solvation, and in order to be able to calculate a

DOI: 10.1021/acs.jctc.5b00484
J. Chem. Theory Comput. 2015, 11, 4780−4790

VSF spectrum in agreement with the experimental observations, the effects of solvation clearly must be included.

Adding microsolvating waters to the structures in the DFT calculations, which provide the vibrational frequencies, polarizabilities, and dipole moments used to calculate the VSF spectra, allows the inclusion of partial solvation effects. The complete set of DFT structures (the structure set) is composed of all combinations of a subset of structures with different molecular conformations (the conformer set) and a subset of structures with different numbers and arrangements of microsolvating waters (the solvation set). The conformer set for PMA monomer units is shown in the black box on the left side of Figure 1. Each monomer unit has two rotatable bonds: the carboxylic acid carbon−tertiary carbon bond and the tertiary carbon−methylene carbon bond. This leads to the nine conformer set structures shown. MD structures are matched to the different conformations by comparison of relevant internal dihedral angles.

The blue box on the right side of Figure 1 contains representations of structures in the solvation set of PMA. The structures vary in the number and arrangement of hydrogen bonds by the addition of microsolvating water molecules. Structures in the solvation set are denoted using a numeric tag that identifies the number of hydrogen bonds between water and each O or H atom in the carboxylic acid group in the order (a) carbonyl oxygen, (b) hydroxyl oxygen, and (c) hydroxyl hydrogen. With the assumption that each oxygen atom can form at most two hydrogen bonds and each hydrogen atom can form at most one hydrogen bond, the solvation set consists of 18 possible hydrogen-bonding arrangements. As is common when analyzing MD trajectories,[45] a simple intermolecular O−H distance threshold (the H-bond cutoff) is used to define hydrogen bonds.

Each structure in the complete DFT structure set is a combination of a single structure in the conformer set with a single structure in the solvation set. The total number of structures in the structure set is therefore the product of the number of structures in the conformer set and the number of structures in the solvation set. A total of 162 structures result from the conformer set and solvation set in Figure 1. The total number of structures is reduced by restricting both the conformer set and the solvation set to only those structures that account for at least 3% of the total population in the MD simulations. This results in a structure set of 36 structures, for both iPMA and sPMA, that spans the most common conformations and solvation states present in the MD trajectories. The reduced solvation set used consists of the six structures displayed in Figure 2.

The populations of the solvation set members in the MD trajectories, however, are dependent on the choice of the H-bond cutoff. Generally, a value above 2.3 Å is used,[45] but the hydrogen bonds in the DFT structures tend to be shorter than 2.0 Å, suggesting that a shorter H-bond cutoff may be more appropriate for matching the MD and DFT structures. Five H-bond cutoff lengths between 1.9 and 2.0 Å were used to assess the sensitivity of the solvation set populations and calculated spectra to the parameter defining a hydrogen bond. Figure 2 shows the percentages of MD structures for iPMA that are matched with the different solvation set structures as a function of the choice of H-bond cutoff distance. The majority of the structures (>98.5%) have between zero and three hydrogen bonds between water molecules and the carboxylic acid moiety. It is clear from the populations in Figure 2 that this remains

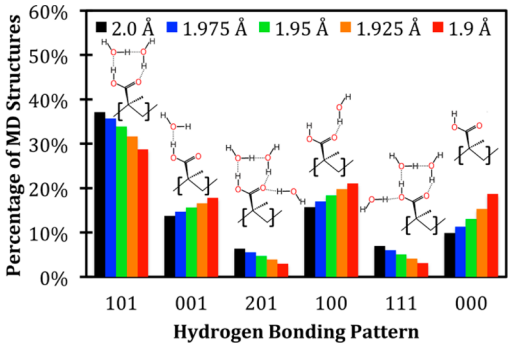

Figure 2. Populations and representative solvation set structures for iPMA as a function of hydrogen bond cutoff length from 2.0 Å (left, in black) to 1.9 Å (right, in red).

true over the studied range of H-bond cutoff distances. The distribution of structures between those that have zero or one hydrogen bonds and those with two or three hydrogen bonds is more strongly affected by changes in the cutoff distance. As the cutoff distance is decreased, the percentage of structures with two or more hydrogen bonds (101, 201, 111) decreases and the number with one or fewer (001, 100, 000) increases. In all cases, the 101 member of the solvation set has the highest population, likely because of the spacing of the hydroxyl hydrogen and carbonyl oxygen, which easily permits cyclic hydrogen-bonding structures with water. Analysis of the sPMA simulations, included in the Supporting Information, shows similar behavior. For the methodology employed here, a H-bond cutoff of 1.975 Å provided the best agreement between the calculated and experimental spectra. Most of the following analysis will therefore be performed using this cutoff value.

A comparison of the total number of hydrogen bonds between water molecules and the carboxylic acid moieties for iPMA and sPMA using the chosen cutoff of 1.975 Å is shown in Figure 3. For both isomers, the most common solvated

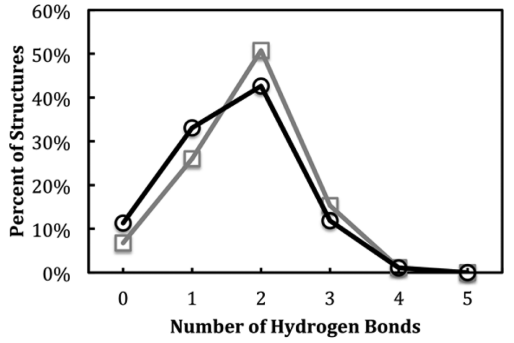

Figure 3. Numbers of hydrogen bonds between water molecules and the carboxylic acid moiety for sPMA (gray squares) and iPMA (black circles).

structures have two hydrogen bonds between water molecules and the carboxylic acid moiety. The isotactic isomer shows fewer contributions from structures with two or three hydrogen bonds (well-solvated) and greater contributions from structures with zero or one hydrogen bond (poorly solvated) compared with the syndiotactic isomer. Overall, the carboxylic acid moieties in iPMA have an average of 1.58 hydrogen bonds to water, while those in sPMA average 1.78. This is in agreement with the experimental spectra, which show signs of weaker solvation of iPMA at the oil/water interface as evidenced by

DOI: 10.1021/acs.jctc.5b00484
J. Chem. Theory Comput. 2015, 11, 4780−4790

comparison of relative VSF spectral intensities of the peaks corresponding to the carbonyl stretching mode.[14]

3.2. Poly(methacrylic acid) SSP Spectra. The specific molecular details behind the differences in the experimental VSF spectra of the two isomers can be obtained from calculations. Calculated VSF spectra for iPMA and sPMA at the oil/water interface are displayed along with fits of experimental spectra (5 ppm, pH 2, SSP polarization) from the literature[14] in Figure 4. The computational methodology

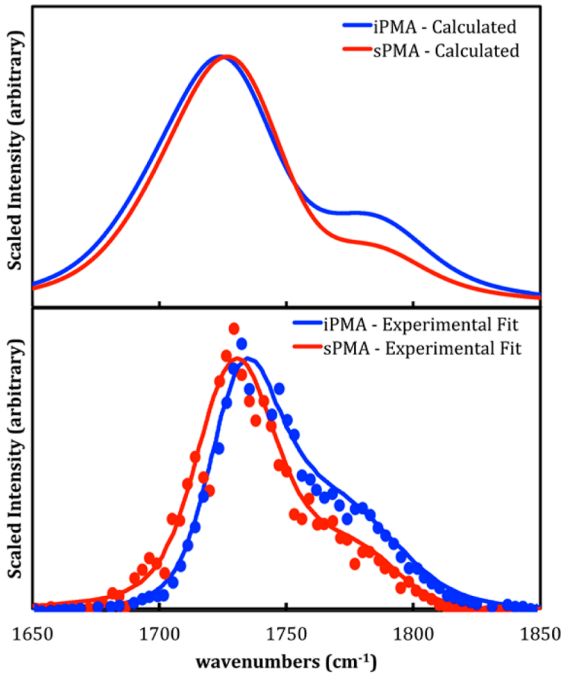

Figure 4. (top) Calculated SSP VSF spectra and (bottom) experimental data points and fits[14] for iPMA (blue) and sPMA (red).

currently includes only spectral contributions from the PMA molecules. Because of the nature of the oil/water interfaces studied, however, nonresonant contributions as well as resonant contributions from the solvent to the experimental spectra are small.[14,46] Thus, the intensities in both the calculated and experimental spectra arise almost exclusively from the vibrational modes of the PMA molecules, allowing direct comparison. In all cases, the spectra have been scaled to the intensity of the peak near 1730 cm^{-1} to permit straightforward visual comparison of features.

The calculated spectra mirror the two main features of the experimental spectra: a dominant peak with a shoulder to the blue of it. The dominant peak in the calculated spectrum is centered near 1725 cm^{-1} and corresponds to the well-solvated structures (101, 201, 111), which have contributions between 1705 and 1745 cm^{-1}. The dominant experimental peaks appear at 1731 cm^{-1} for sPMA and 1734 cm^{-1} for iPMA. A strong shoulder appears near 1770 cm^{-1} in both the calculated and experimental spectra. Structures that are poorly solvated (100, 001, 000) contribute to the intensity from 1750 to 1800 cm^{-1}. In the calculations, the frequency difference between the peak corresponding to well-solvated structures and the peak corresponding to poorly solvated structures is slightly overestimated compared with the experimental spectrum. The overestimation of the separation may be a consequence of representing the continuum of dynamic solvation states with the static structures in the structure set.

The intensities of VSF spectra are dependent on both molecular orientation and population. In simple systems, these contributions can be decoupled using techniques that provide a measure of surface population, such as surface tensiometry. Currently, only theoretical calculations can serve to elucidate the populations and orientations of interfacial species in varying solvation environments. Population analysis of the molecular dynamics trajectories shows a ratio of 44 poorly solvated to 54 well-solvated structures for iPMA and a 33:66 ratio for sPMA. The relative intensities of the two main peaks in the spectra are 21:54 for iPMA and 16:66 for sPMA. From the solvation structure ratios and the relative intensities of the peaks in the final convoluted spectra, it can be inferred that the well-solvated carboxylic acid groups contribute twice as much intensity per moiety as their poorly solvated counterparts. Under the assumption that the contributing vibrational response tensors are only marginally affected by the presence of the microsolvating waters, the difference in contribution per moiety must arise from differences in the degree of orientational anisotropy of the molecules. This suggests that the well-solvated structures are more strongly oriented than the poorly solvated structures.

3.3. Glutaric Acid Solvation Structures. The approach outlined for calculating VSF spectra of strongly solvated modes was also leveraged for glutaric acid, a five-carbon straight-chain dicarboxylic acid, at the air/water interface. Glutaric acid is a member of a unique class of surface-active molecules composed of a hydrophobic and flexible aliphatic chain capped by hydrophilic moieties (carboxylic acid groups). Solvation of the carboxylic acid moieties follows a fairly different pattern compared with that seen in the case of the PMA isomers. The carboxylic acid moieties in glutaric acid are slightly more strongly solvated than those in the PMA isomers, with >96.6% of the structures having between zero and three hydrogen bonds with water molecules. Figure 5 presents the percentages of MD structures corresponding to different solvation structures as a function of the H-bond cutoff distance.

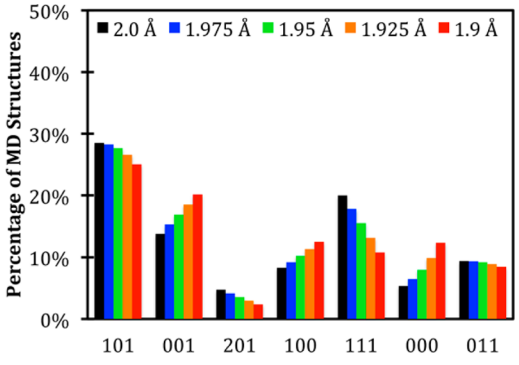

Figure 5. Populations of solvation patterns for glutaric acid as a function of hydrogen bond cutoff length from 2.0 Å (left, in black) to 1.9 Å (right, in red).

As was the case with the PMA polymers, the most common solvation set structure is the 101 structure with hydrogen bonds to the hydroxyl H and the carbonyl O. Structures with a single hydrogen bond involving these atoms are also prevalent. However, solvation set structures involving hydrogen bonding to the hydroxyl O account for a much greater portion of the structures than with either PMA isomer. This may be a

DOI: 10.1021/acs.jctc.5b00484
J. Chem. Theory Comput. 2015, 11, 4780−4790

consequence of the decreased bulk of the molecular structure adjacent to the carboxylic acid groups in glutaric acid. In the PMA polymers, the carboxylic acid group is bound to a quaternary carbon. In glutaric acid, the carboxylic moieties are attached to secondary carbons, leading to greatly reduced steric hindrance for water molecules that are hydrogen-bonded to the hydroxyl oxygens. Variations due to the choice of cutoff for defining a hydrogen bond follow the same trends as seen with the polymers. The populations of structures with two or more hydrogen bonds (101, 201, 111, 011) decrease and those of structures with one or fewer hydrogen bonds (001, 100, 000) increase as the cutoff length is reduced.

For a hydrogen bond cutoff length of 1.975 Å, the percentages of carboxylic acid moieties with certain numbers of hydrogen bonds are shown in Figure 6. The majority of

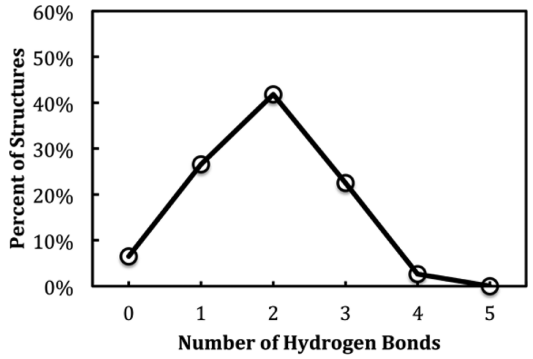

Figure 6. Distribution of the numbers of hydrogen bonds between water molecules and each carboxylic acid moiety for glutaric acid.

structures (~91%) have between one and three hydrogen bonds to each carboxylic acid group. The distribution shows increased contributions from structures with two or three hydrogen bonds compared with either PMA polymer. The average number of hydrogen bonds is 1.88 per carboxylic acid moiety.

3.4. Glutaric Acid SSP Spectrum. The calculated SSP VSF spectrum of glutaric acid in the carbonyl stretching region is shown in Figure 7 along with the experimental fit from ref 31.

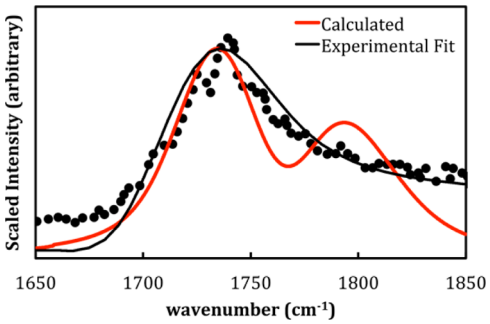

Figure 7. Calculated SSP VSF spectrum (red) and experimental data points and fit (black)[31] for glutaric acid.

Unlike the oil/water interface, in VSF spectra of the air/water interface in the carbonyl stretching region there are generally non-negligible intensity contributions due to water bending modes and nonresonant considerations. Thus, the VSF spectrum calculated here, which does not include spectral intensity contributions from water modes, is not expected to completely reproduce the features and line shapes present in the experimental spectrum. The calculated spectrum was generated using a hydrogen bond cutoff distance of 1.975 Å, as determined to be best previously. Both the calculated and experimental spectra have their dominant peak at ~1730 cm^{-1}. The calculated spectrum has a secondary peak centered at ~1790 cm^{-1}, while the experimental spectrum has a strong tail in this region, likely due to a combination of contributions from carbonyl stretching as well as water bending modes and/or interference with the nonresonant background, as shown in recent experimental work.[31] The calculated spectrum is a great improvement on the spectrum calculated without including microsolvating waters in the DFT structures (but with anharmonic frequencies), which has a single symmetric feature at ~1770 cm^{-1}.

The calculated VSF spectrum can be analyzed to determine the solvation set structures associated with each portion of the spectrum. Much like previous studies,[47−49] the vibrational frequency of the carbonyl stretching mode of the carboxylic acid moiety is dependent on the number of hydrogen bonds it is experiencing. The calculations here show that the carbonyl stretching frequency is affected not only by hydrogen bonds to the carbonyl oxygen but also by hydrogen bonds involving the hydroxyl hydrogen and oxygen. Hydrogen bonds to the carbonyl oxygen and hydroxyl hydrogen both draw electron density from the C═O bond, leading to a shift to lower frequencies. A shift to higher frequencies occurs for solvation structures with a hydrogen bond to the hydroxyl oxygen, as electron density is drawn from the central carbon atom, causing the C═O bond to strengthen.

The major peak at 1730 cm^{-1} corresponds to the 101 solvation structures. Moving toward higher wavenumbers, there are contributions from the 111 structures near 1750 cm^{-1}, from the 001 structures between 1760 and 1775 cm^{-1}, from the 011 structures near 1775 cm^{-1}, and from the 100 structures near 1790 cm^{-1}. The strong connection between the solvation set structure and the corresponding shift of the carbonyl stretching frequency is similar for glutaric acid and the PMA polymers. General frequency ranges for the different solvation set structures, which are applicable to all of the molecules studied here, are shown in Table 1.

Table 1. Carboxylic Acid C═O Stretching Frequencies for Common Solvation Set Structures

solvation set structure	calculated vibrational frequency range
100	1773−1793 cm^{-1}
001	1758−1781 cm^{-1}
101	1725−1742 cm^{-1}
011	1770−1801 cm^{-1}
111	1735−1757 cm^{-1}
201	1696−1718 cm^{-1}
211	1727−1729 cm^{-1}

The information regarding the dependence of the vibrational frequencies on the solvation state contained in Table 1 would be sufficient for interpretation of spectra obtained with incoherent spectroscopic techniques. The coherent nature of VSF spectroscopy requires computational methodology that provides not only accurate vibrational frequencies but also considers interfacial populations and molecular orientations. The methodology presented here provides all of the requisite information and is capable of generating accurate VSF spectra that consider solvation effects for a relatively low computational

DOI: 10.1021/acs.jctc.5b00484
J. Chem. Theory Comput. 2015, 11, 4780−4790

cost. To gauge the limits of this methodology, however, a more detailed understanding of the sensitivities of the calculated spectra to the choice of H-bond cutoff distance, solvation set, and conformer set is required. The following sections will investigate the dependence of the spectra on each of these components.

3.5. Effect of the H-Bond Cutoff on the VSF Spectrum. The calculated VSF spectra are sensitive both to the choice of the H-bond cutoff distance and the choice of structures that are included in the description of the MD continuum. Additionally, the sensitivity of the spectra to changes in one of these choices is correlated to the sensitivity of the spectra to changes in the other. The analysis here alters each of the variables independently, leaving the other fixed at the value used to achieve the spectra in Figures 4 and 7.

The sensitivity to the H-bond cutoff length is shown for the three molecular species of interest (iPMA, sPMA, and glutaric acid) in Figure 8. All of the spectra have been normalized to the

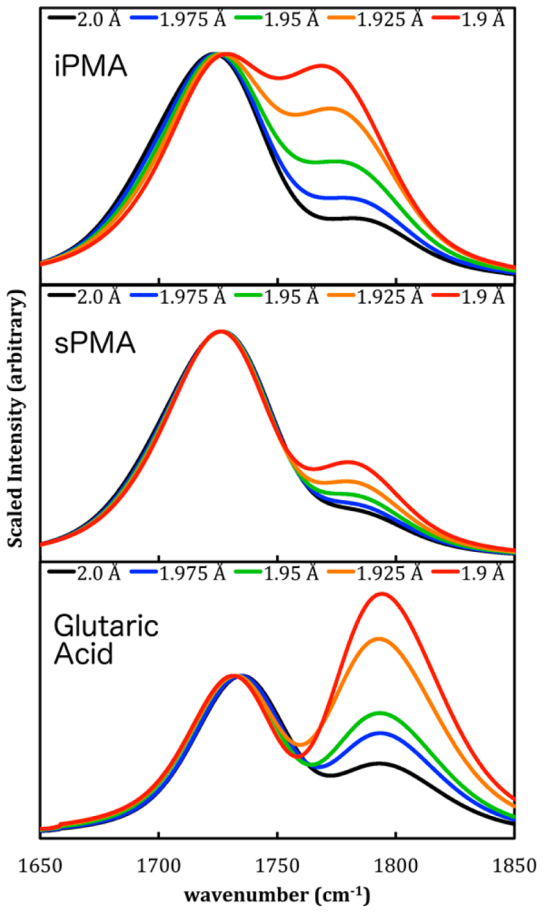

Figure 8. Calculated VSF spectra using the original structure set and various H-bond cutoff distances. Results are shown for (top) iPMA, (middle) sPMA, and (bottom) glutaric acid with H-bond cutoffs of 2.0 Å (black), 1.975 Å (blue), 1.95 Å (green), 1.925 Å (orange), and 1.9 Å (red).

intensity of the peak at ∼1730 cm^{-1}. As the cutoff is increased from 1.9 to 2.0 Å, contributions to the spectra from the poorly solvated structures become more prominent. For glutaric acid and iPMA, the increase in the intensity of the higher-frequency peak at ∼1770−1790 cm^{-1} due to these structures is substantial, causing it to surpass the peak at ∼1730 cm^{-1} as the dominant peak for glutaric acid for the shortest H-bond cutoffs. In contrast, the sPMA spectrum shows minimal change as the cutoff is varied.

The difference in behavior can be explained by examining the populations of the solvated species that contribute to each peak in the spectra. The feature at ∼1730 cm^{-1} has contributions from well-solvated carboxylic acid groups (101, 111, 201). The high-wavenumber peaks have contributions from poorly solvated carboxylic acid groups (001, 100, 000) as well as the 011 solvation structures in the case of glutaric acid. It might be expected that the calculated spectra of molecules with similar degrees of solvation would have similar changes when the cutoff is altered. Comparison of the average numbers of hydrogen bonds per carboxylic acid moiety determined from the MD calculations (1.88 for glutaric acid, 1.78 for sPMA, and 1.58 for iPMA) clearly shows that this is not the case. Since sPMA is more strongly solvated than iPMA and their spectra calculated with a cutoff of 1.975 Å are similar, it is expected that iPMA will be more sensitive to changes in the H-bond cutoff. The observed sensitivities for sPMA and iPMA are indeed found to be quite different, consistent with the large difference in the average numbers of hydrogen bonds per moiety for the two species.

The changes in the glutaric acid spectrum, however, are similar to those seen with iPMA even though the average number of hydrogen bonds for a carboxylic acid group in glutaric acid is closer to the sPMA value than the iPMA value. The fact that the 011 solvation set structure (with one H-bond to the hydroxyl oxygen and one H-bond to the hydroxyl hydrogen) contributes to the poorly solvated peak for glutaric acid causes this discrepancy. To gain insight as to why this is true, the ratio of populations of the two groups of solvation set structures that correspond to the two peaks in each spectrum were compared. Additionally, the ratio was calculated for glutaric acid discounting the 011 structures. For iPMA, the poorly solvated:well-solvated ratio ranges from 3:4 for the 2.0 Å cutoff to 5:3 for the 1.9 Å cutoff. This is similar to the range of ratios seen with glutaric acid (2:3 and 3:2, respectively), which clarifies why the glutaric acid and iPMA spectra respond similarly to changes in the H-bond cutoff. In contrast, the ratio ranges from 4:9 to 8:9 for sPMA. Removal of the contributions of the 011 solvation structures for glutaric acid gives ratios of 1:2 and 6:5, which are much closer to the ratios seen for sPMA. The 011 solvation set structures have more than the average number of hydrogen bonds (2 vs 1.88) but have vibrational frequencies closer to the peak corresponding to poorly solvated structures. The increased presence of these structures in the glutaric acid MD trajectories compared with the PMA MD trajectories is the cause of the unexpected behavior as a function of the H-bond cutoff length.

Variation of the H-bond cutoff distance also reveals that the calculated spectra are not strongly impacted by small variations from the typical literature value of 2.0 Å. Cutoffs between 1.95 and 2.0 Å all generate spectra in reasonable agreement with the experimental relative peak intensities. Deviations from the experimental fits grow quickly as the cutoff is reduced below 1.95 Å, with the number of structures defined as poorly solvated greatly increasing. Results for cutoffs above 2.0 Å, which are not shown, underestimate the intensity of the poorly solvated peak. The optimal H-bond cutoff likely depends on the system studied, the MD force field and parameters, and the choice of DFT conformational and solvation structures. The flexibility of the choice of cutoff, however, means that choosing

DOI: 10.1021/acs.jctc.5b00484
J. Chem. Theory Comput. 2015, 11, 4780−4790

a reasonable H-bond cutoff (between 1.95 and 2.0 Å) will be able to provide predictive spectra.

3.6. Effect of the Choice of Solvation Set Structures. The effect of altering the choice of structures composing the structure set is expected to be less straightforward than the effect of changing the H-bond cutoff. Unfortunately, it is not clear that simply adding more structures will always provide better results, though it will always prove more computationally expensive. Because of the different populations of the different conformer set/solvation set structures in the MD trajectories, structures that are less common are less well sampled than those that are more common. This relationship holds except in the limit of prohibitively long MD evolutions, where even the least common structures have adequately sampled the available orientational space. A consequence of this difference in sampling is that structures with smaller populations can give rise to erroneous spectral contributions. Additionally, there are concerns over computational expense for molecular systems with a large number of internal degrees of freedom and/or a large number of hydrogen-bonding sites. Removing structures below a certain population from consideration in the calculations served to address these issues previously,[14,31] and similar methodology has been applied in the spectra shown above.

Here the effect of the number of structures included in the solvation set is examined. Figure 9 shows the calculated spectra

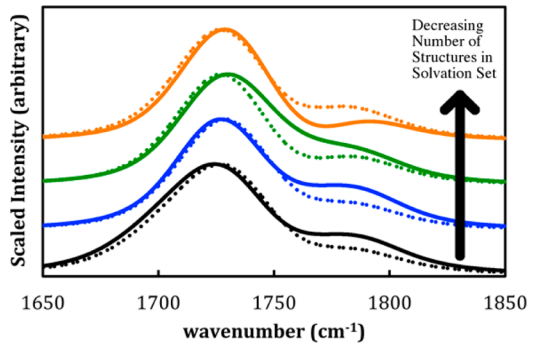

Figure 9. Calculated SSP VSF spectra of iPMA (solid) and sPMA (dotted) with solvation set C (orange), solvation set B (green), solvation set A (blue), and the original solvation set (black). The spectra have been offset for clarity.

of iPMA (solid lines) and sPMA (dotted lines) as the number of solvation set components is reduced. The conformer set was not altered. The initial solvation set included the same structures as the solvation set used to generate the spectra in Figure 4 (i.e., 101, 001, 100, 000, 111, and 201) and included all structures that constituted more than 2.5% of the total population. These were systematically removed in order of lowest population in the MD calculations using a 1.975 Å hydrogen bond cutoff. The reduced solvation sets considered therefore include solvation set A (the 101, 001, 100, 000, and 111 structures), solvation set B (the 101, 001, 100, and 000 structures), and solvation set C (the 101, 001, and 100 structures).

The removal of the 201 structures from the solvation set (original set to set A) removes all of the spectral contributions at ~1710 cm^{-1}. The dominant peak becomes narrower as a result. Removal of the remaining solvation set structures mainly affects the iPMA spectrum. The relative intensities in the sPMA spectrum remain essentially unchanged in this range of structure sets because the solvation set structures removed do not substantially alter the ratio of well and poorly solvated structures. Removal of the 111 structures (set A to set B) is more impactful, especially in regard to the shape of the iPMA spectrum, as the ratio of well and poorly solvated structures is quite different from the ratio using the original solvation set. Still, the iPMA spectrum shows a stronger secondary peak than the sPMA spectrum does, in agreement with the experimental measurements. When the 000 structures are removed from the structure set (set B to set C), the secondary peak of the sPMA spectrum is stronger than that of the iPMA spectrum, which is inconsistent with experiment. From this it is clear that the structures composing set C are not sufficient for calculation of reasonable spectra for the PMA polymers. Further reduction eliminates any resemblance between the calculated and experimental spectra for both PMA polymers.

In the case of glutaric acid, the original solvation set used to calculate the spectrum in Figure 7 includes any solvation structure that constituted over 2% of the total population for any of the H-bond cutoffs (between 1.9 and 2.0 Å). Considering the solvation set with the resulting 19 components and the conformer set including the seven most populous molecular conformations, the original structure set includes 133 DFT structures. With the scheme employed here, the 324 possible solvation set structures and 25 possible conformations would generate a structure set containing 8100 DFT structures. Even though the original structure set used contains 60 times fewer structures than the total possible, the solvation set encompasses over 55% of the solvation states, and the conformer set includes over 75% of the conformations present in the MD calculations.

Figure 10 shows the effect of reducing the number of solvation set structures considered when generating the

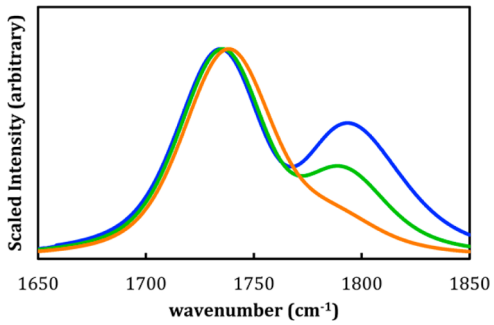

Figure 10. Calculated SSP VSF spectra of glutaric acid with the set OG (blue), set 2G (green), and set 4G (orange) solvation sets.

structure set. It compares the original solvation set (set OG) to solvation sets containing solvation structures that contribute greater than 2% (set 2G) and greater than 4% (set 4G) of structures in the MD trajectories considering a 1.975 Å hydrogen bond cutoff. Population percentage cutoffs are used in this case because there are a greater number of structures than in the PMA studies and the glutaric acid structures include solvation at all six potential hydrogen-bonding sites. All of the sets use the original conformer set (seven conformers), leading to 91 total structures for set 2G and 35 total structures for set 4G. Reducing the number of solvation set structures has the opposite effect that reducing the hydrogen bond cutoff does. Mainly, the intensity of the higher-wavenumber peak is reduced

DOI: 10.1021/acs.jctc.5b00484
J. Chem. Theory Comput. 2015, 11, 4780−4790

relative to that of the dominant peak. This is especially evident with set 4G.

For both PMA and glutaric acid, reducing the number of structures in the solvation set and reducing the hydrogen bond cutoff distance have inverse effects on the spectra, which may be an additional explanation for why the optimal hydrogen bond cutoff was found to be below the commonly used values above 2.3 Å. Figures 9 and 10 show that use of incomplete solvation sets leads to overestimation of the relative intensity of the well-solvated peak. This effect can be countered by reducing the H-bond cutoff, which tends to cause underestimation of the relative intensity of the well-solvated peak. It might therefore be possible to generate reasonably accurate spectra with very small solvation sets by greatly reducing the H-bond cutoff, but caution should be exercised. Here, a combination of a set of solvation structures with a greater than 2% population in the MD calculations and a hydrogen bond cutoff of 1.975 Å performs well. However, the poor agreement with experiment attained with a smaller set of structures, such as used for iPMA and glutaric acid in Figures 9 and 10, may be offset by further reducing the hydrogen bond cutoff distance. This approach would have practical limits in the minimum number of structures in the solvation set or minimum H-bond cutoff but may serve as a possible way to generate VSF spectra for very large and complex molecules at interfaces.

An additional way to treat systems with a larger number of degrees of freedom is to reduce the number of structures in the conformer set. If it is assumed that the spectrum of the most common conformer is representative, the number of DFT structures can be greatly reduced. Such a reduction was performed for glutaric acid using the set OG, set 2G, and set 4G solvation sets for only the most common conformer to produce structure sets OG1, 2G1, and 4G1. The resulting spectra are shown in Figure 11. Use of only the most common conformer in the conformer set was found to be a reasonable approximation in this case, as only minor differences exist compared to the calculated spectra in Figure 10, where a larger conformer set was used. A similar approach would not be valid when calculating spectra of the CH stretching modes, where multiple conformers are necessary to generate an accurate spectrum.[31]

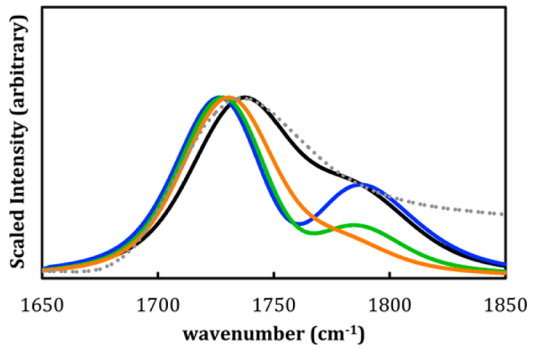

Figure 11. Calculated SSP VSF spectra of glutaric acid using a single conformer with various solvation sets, giving structure sets OG1 (blue), 2G1 (green), 4G1 (orange), and set EXT (black). The experimental fit from ref 31 is shown by the gray dotted line.

Reducing the number of conformers makes it more reasonable to extend the number of structures in the solvation set considered in generating the DFT structure set. The spectrum calculated using such a solvation set (set EXT) is also shown in Figure 11. Instead of using a simple population percentage cutoff, structures in set EXT were chosen (starting with the most populous in each group with the same number of hydrogen bonds) to mimic the relative populations of the hydrogen-bonding populations in Figure 7. The solvation set determined in this way consists of 34 structures. The resulting spectrum has increased intensity near 1760 cm^{-1} and seems to more closely match the experimental spectrum. The uncertainty in the relative contributions from the glutaric acid resonant modes and other contributions prevents further comparison. Comparisons for determining a best approach to picking a solvation set for glutaric acid will require experimental spectra in D_2O, extension of the computational methodology, or calculation of spectra for additional systems.

4. CONCLUSIONS

Vibrational sum-frequency spectra for two poly(methacrylic acid) stereoisomers at an oil/water interface and glutaric acid at an air/water interface were calculated by combining pertinent information from classical molecular dynamics and density functional theory calculations. Effects of solvation by water were taken into account by microsolvation of the DFT structures with water molecules. When only solvation patterns comprising more than ∼2% of the total population of the structures in the MD trajectories were considered, as was done with the original solvation structure sets, a hydrogen bond length cutoff definition of 1.975 Å was found to provide a fairly accurate reproduction of the experimental spectra. In all cases, the most common solvation state of the carboxylic acid moieties involves two hydrogen bonds to the carbonyl moiety, one to the carbonyl oxygen and one to the carboxylic acid hydrogen. The calculated spectra were found to be only mildly sensitive to moderate changes in the hydrogen bond length cutoff and in which DFT structures were included. Reduction of the hydrogen bond length cutoff led to an increase in the relative intensity of peaks corresponding to poorly solvated carboxylic acid groups. Reducing the number of solvation structures included in the DFT structure set resulted in increased relative contributions from the more well solvated structures. The methodology introduced here has been shown to be capable of calculating reasonably accurate VSF spectra involving vibrational modes that are strongly dependent on the solvation environment with minimal extra computational expense. The method has also proved to be quite robust in regard to changes in the calculation parameters, making it ideal for the calculation of predictive VSF spectra of complex and large molecular systems even when solvation plays a role.

■ ASSOCIATED CONTENT

Supporting Information

The Supporting Information is available free of charge on the ACS Publications website at DOI: 10.1021/acs.jctc.5b00484.

Populations for sPMA as a function of hydrogen bond cutoff length and selected density functional theory geometries and vibrational frequencies (PDF)

■ AUTHOR INFORMATION

Corresponding Author

*E-mail: richmond@uoregon.edu.

Funding

The authors are grateful for financial support for this work from NSF Grant CHE-1051215.

DOI: 10.1021/acs.jctc.5b00484
J. Chem. Theory Comput. 2015, 11, 4780−4790

Notes

The authors declare no competing financial interest.

■ ACKNOWLEDGMENTS

The authors thank Laura McWilliams and Dr. Sumi Wren for assistance with the manuscript.

■ REFERENCES

(1) Johnson, M.; Baldelli, S. Vibrational Sum Frequency Spectroscopy Studies of the Influence of Solutes and Phospholipids at Vapor/Water Interfaces Relevant to Biological and Environmental Systems. *Chem. Rev.* **2014**, *114*, 8416−8446.

(2) Jubb, A. M.; Hua, W.; Allen, H. C. Organization of Water and Atmospherically Relevant Ions and Solutes: Vibrational Sum Frequency Spectroscopy at the Vapor/Liquid and Liquid/Solid Interfaces. *Acc. Chem. Res.* **2012**, *45*, 110−119.

(3) Shrestha, M.; Zhang, Y.; Ebben, C. J.; Martin, S. T.; Geiger, F. M. Vibrational Sum Frequency Generation Spectroscopy of Secondary Organic Material Produced by Condensational Growth from α-Pinene Ozonolysis. *J. Phys. Chem. A* **2013**, *117*, 8427−8436.

(4) Wren, S. N.; Gordon, B. P.; Valley, N. A.; McWilliams, L. E.; Richmond, G. L. Hydration, Orientation, and Conformation of Methylglyoxal at the Air-Water Interface. *J. Phys. Chem. A* **2015**, *119*, 6391−6403.

(5) Plath, K. L.; Valley, N. A.; Richmond, G. L. Ion-Induced Reorientation and Distribution of Pentanone in the Air-Water Boundary Layer. *J. Phys. Chem. A* **2013**, *117*, 11514−11527.

(6) Blower, P. G.; Shamay, E.; Kringle, L.; Ota, S. T.; Richmond, G. L. Surface Behavior of Malonic Acid Adsorption at the Air/Water Interface. *J. Phys. Chem. A* **2013**, *117*, 2529−2542.

(7) Johnson, C. M.; Tyrode, E.; Baldelli, S.; Rutland, M. W.; Leygraf, C. A Vibrational Sum Frequency Spectroscopy Study of the Liquid−Gas Interface of Acetic Acid−Water Mixtures: 1. Surface Speciation. *J. Phys. Chem. B* **2005**, *109*, 321−328.

(8) Ota, S. T.; Richmond, G. L. Uptake of SO_2 to Aqueous Formaldehyde Surfaces. *J. Am. Chem. Soc.* **2012**, *134*, 9967−9977.

(9) Ma, G.; Allen, H. C. Surface Studies of Aqueous Methanol Solutions by Vibrational Broad Bandwidth Sum Frequency Generation Spectroscopy. *J. Phys. Chem. B* **2003**, *107*, 6343−6349.

(10) Lu, R.; Gan, W.; Wu, B. H.; Zhang, Z.; Guo, Y.; Wang, H. F. C−H Stretching Vibrations of Methyl, Methylene and Methine Groups at the Vapor/Alcohol (n = 1−8) Interfaces. *J. Phys. Chem. B* **2005**, *109*, 14118−14129.

(11) Tyrode, E.; Johnson, C. M.; Baldelli, S.; Leygraf, C.; Rutland, M. W. A Vibrational Sum Frequency Spectroscopy Study of the Liquid−Gas Interface of Acetic Acid−Water Mixtures: 2. Orientation Analysis. *J. Phys. Chem. B* **2005**, *109*, 329−341.

(12) Johnson, C. M.; Tyrode, E.; Kumpulainen, A.; Leygraf, C. Vibrational Sum Frequency Spectroscopy Study of the Liquid/Vapor Interface of Formic Acid/Water Solutions. *J. Phys. Chem. C* **2009**, *113*, 13209−13218.

(13) Beaman, D. K.; Robertson, E. J.; Richmond, G. L. Ordered Polyelectrolyte Assembly at the Oil−Water Interface. *Proc. Natl. Acad. Sci. U. S. A.* **2012**, *109*, 3226−3231.

(14) Valley, N. A.; Robertson, E. J.; Richmond, G. L. Twist and Turn: Effect of Stereoconfiguration on the Interfacial Assembly of Polyelectrolytes. *Langmuir* **2014**, *30*, 14226−14233.

(15) Chen, Z.; Shen, Y. R.; Somorjai, G. A. Studies of Polymer Surfaces by Sum Frequency Generation Vibrational Spectroscopy. *Annu. Rev. Phys. Chem.* **2002**, *53*, 437−465.

(16) Lambert, A. G.; Davies, P. B.; Neivandt, D. J. Implementing the theory of sum frequency generation vibrational spectroscopy: A tutorial review. *Appl. Spectrosc. Rev.* **2005**, *40*, 103−145.

(17) Shen, Y. R. Basic Theory of Surface Sum-Frequency Generation. *J. Phys. Chem. C* **2012**, *116*, 15505−15509.

(18) Morita, A.; Hynes, J. T. A Theoretical Analysis of the Sum Frequency Generation Spectrum of the Water Surface. *Chem. Phys.* **2000**, *258*, 371−390.

(19) Sulpizi, M.; Salanne, M.; Sprik, M.; Gaigeot, M.-P. Vibrational Sum Frequency Generation Spectroscopy of the Water Liquid−Vapor Interface from Density Functional Theory-Based Molecular Dynamics Simulations. *J. Phys. Chem. Lett.* **2013**, *4*, 83−87.

(20) Ishiyama, T.; Takahashi, H.; Morita, A. Vibrational Spectrum at a Water Surface: A Hybrid Quantum Mechanics/Molecular Mechanics Molecular Dynamics Approach. *J. Phys.: Condens. Matter* **2012**, *24*, 124107.

(21) Morita, A.; Hynes, J. T. A Theoretical Analysis of the Sum Frequency Generation Spectrum of the Water Surface. II. Time-Dependent Approach. *J. Phys. Chem. B* **2002**, *106*, 673−685.

(22) Morita, A. Improved Computation of Sum Frequency Generation Spectrum of the Surface of Water. *J. Phys. Chem. B* **2006**, *110*, 3158−3163.

(23) Nagata, Y.; Mukamel, S. Vibrational Sum-Frequency Generation Spectroscopy at the Water/Lipid Interface: Molecular Dynamics Simulation Study. *J. Am. Chem. Soc.* **2010**, *132*, 6434−6442.

(24) Brown, M. G.; Walker, D. S.; Raymond, E. A.; Richmond, G. L. Vibrational Sum-Frequency Spectroscopy of Alkane/Water Interfaces: Experiment and Theoretical Simulation. *J. Phys. Chem. B* **2003**, *107*, 237−244.

(25) Ishiyama, T.; Imamura, T.; Morita, A. Theoretical Studies of Structures and Vibrational Sum Frequency Generation Spectra at Aqueous Interfaces. *Chem. Rev.* **2014**, *114*, 8447−8470.

(26) Ishiyama, T.; Sato, Y.; Morita, A. Interfacial Structures and Vibrational Spectra at Liquid/Liquid Boundaries: Molecular Dynamics Study of Water/Carbon Tetrachloride and Water/1,2-Dichloroethane Interfaces. *J. Phys. Chem. C* **2012**, *116*, 21439−21446.

(27) Kawaguchi, T.; Shiratori, K.; Henmi, Y.; Ishiyama, T.; Morita, A. Mechanisms of Sum Frequency Generation from Liquid Benzene: Symmetry Breaking at Interface and Bulk Contribution. *J. Phys. Chem. C* **2012**, *116*, 13169−13182.

(28) Liu, S.; Fourkas, J. T. Orientational Time Correlation Functions for Vibrational Sum-Frequency Generation. 2. Propionitrile. *J. Phys. Chem. B* **2014**, *118*, 8406−8419.

(29) Liu, S.; Fourkas, J. T. Orientational Time Correlation Functions for Vibrational Sum-Frequency Generation. 2. Acetonitrile. *J. Phys. Chem. A* **2013**, *117*, 5853−5864.

(30) Ishiyama, T.; Sokolov, V. V.; Morita, A. Molecular Dynamics Simulation of Liquid Methanol. II. Unified Assignment of Infrared, Raman, and Sum Frequency Generation Vibrational Spectra in Methyl C−H Stretching Region. *J. Chem. Phys.* **2011**, *134*, 024510.

(31) Valley, N. A.; Blower, P. G.; Wood, S. R.; Plath, K. L.; McWilliams, L. E.; Richmond, G. L. Doubling Down: Delving into the Details of Diacid Adsorption at Aqueous Surfaces. *J. Phys. Chem. A* **2014**, *118*, 4778−4789.

(32) Roy, S.; Naka, T. L.; Hore, D. K. Enhanced Understanding of Amphipathic Peptide Adsorbed Structure by Modeling of the Nonlinear Vibrational Response. *J. Phys. Chem. C* **2013**, *117*, 24955−24966.

(33) Jerman, B.; Breznik, M.; Kogej, K.; Paoletti, S. Osmotic and Volume Properties of Stereoregular Poly(Methacrylic Acids) in Aqueous Solution: Role of Intermolecular Association. *J. Phys. Chem. B* **2007**, *111*, 8435−8443.

(34) Jerman, B.; Kogej, K. Fluorimetric and Potentiometric Study of the Conformational Transition of Isotactic and Atactic Poly-(methacrylic acid) in Mixed Solvents. *Acta Chim. Slov.* **2006**, *53*, 264−273.

(35) Vlachy, N.; Dolenc, J.; Jerman, B.; Kogej, K. Influence of Stereoregularity of the Polymer Chain on Interactions with Surfactants: Binding of Cetylpyridinium Chloride by Isotactic and Atactic Poly(Methacrylic Acid). *J. Phys. Chem. B* **2006**, *110*, 9061−9071.

(36) Jerman, B.; Podlipnik, C.; Kogej, K. Molecular Dynamics Simulation of Poly(methacrylic acid) Chains in Water. *Acta Chim. Slov.* **2007**, *54*, 509−516.

(37) Case, D. A.; Darden, T. A.; Cheatham, T. E., III; Simmerling, C. L.; Wang, J.; Duke, R. E.; Luo, R.; Walker, R. C.; Zhang, W.; Merz, K. M.; Roberts, B.; Hayik, S.; Roitberg, A.; Seabra, G.; Swails, J.; Götz, A.

DOI: 10.1021/acs.jctc.5b00484
J. Chem. Theory Comput. 2015, 11, 4780−4790

W.; Kolossváry, I.; Wong, K. F.; Paesani, F.; Vanicek, J.; Wolf, R. M.; Liu, J.; Wu, X.; Brozell, S. R.; Steinbrecher, T.; Gohlke, H.; Cai, Q.; Ye, X.; Wang, J.; Hsieh, M.-J.; Cui, G.; Roe, D. R.; Mathews, D. H.; Seetin, M. G.; Salomon-Ferrer, R.; Sagui, C.; Babin, V.; Luchko, T.; Gusarov, S.; Kovalenko, A.; Kollman, P. A. *Amber12*; University of California: San Francisco, 2012.

(38) Martinez, L.; Andrade, R.; Birgin, E.; Martinez, J. PACKMOL: A Package for Building Initial Configurations for Molecular Dynamics Simulations. *J. Comput. Chem.* **2009**, *30*, 2157−2164.

(39) Valiev, M.; Bylaska, E. J.; Govind, N.; Kowalski, K.; Straatsma, T. P.; Van Dam, H. J. J.; Wang, D.; Nieplocha, J.; Apra, E.; Windus, T. L.; de Jong, W. A. NWChem: A Comprehensive and Scalable Open-Source Solution for Large Scale Molecular Simulations. *Comput. Phys. Commun.* **2010**, *181*, 1477−1489.

(40) Bryantsev, V. S.; Diallo, M. S.; van Duin, A. C. T.; Goddard, W. A., III Evaluation of B3LYP, X3LYP, and M06-Class Density Functionals for Predicting the Binding Energies of Neutral, Protonated, and Deprotonated Water Clusters. *J. Chem. Theory Comput.* **2009**, *5*, 1016−1026.

(41) Frisch, M. J.; Trucks, G. W.; Schlegel, H. B.; Scuseria, G. E.; Robb, M. A.; Cheeseman, J. R.; Scalmani, G.; Barone, V.; Mennucci, B.; Petersson, G. A.; Nakatsuji, H.; Caricato, M.; Li, X.; Hratchian, H. P.; Izmaylov, A. F.; Bloino, J.; Zheng, G.; Sonnenberg, J. L.; Hada, M.; Ehara, M.; Toyota, K.; Fukuda, R.; Hasegawa, J.; Ishida, M.; Nakajima, T.; Honda, Y.; Kitao, O.; Nakai, H.; Vreven, T.; Montgomery, J. A., Jr.; Peralta, J. E.; Ogliaro, F.; Bearpark, M.; Heyd, J. J.; Brothers, E.; Kudin, K. N.; Staroverov, V. N.; Kobayashi, R.; Normand, J.; Raghavachari, K.; Rendell, A.; Burant, J. C.; Iyengar, S. S.; Tomasi, J.; Cossi, M.; Rega, N.; Millam, J. M.; Klene, M.; Knox, J. E.; Cross, J. B.; Bakken, V.; Adamo, C.; Jaramillo, J.; Gomperts, R.; Stratmann, R. E.; Yazyev, O.; Austin, A. J.; Cammi, R.; Pomelli, C.; Ochterski, J. W.; Martin, R. L.; Morokuma, K.; Zakrzewski, V. G.; Voth, G. A.; Salvador, P.; Dannenberg, J. J.; Dapprich, S.; Daniels, A. D.; Farkas, Ö.; Foresman, J. B.; Ortiz, J. V.; Cioslowski, J.; Fox, D. J. *Gaussian 09*, revision C; Gaussian, Inc: Wallingford, CT, 2009.

(42) Marechal, Y. IR Spectra of Carboxylic Acids in the Gas Phase: A Quantitative Reinvestigation. *J. Chem. Phys.* **1987**, *87*, 6344−6353.

(43) Bain, C. D. Sum-Frequency Vibrational Spectroscopy of the Solid/Liquid Interface. *J. Chem. Soc., Faraday Trans.* **1995**, *91*, 1281−1296.

(44) Lim, M.; Hochstrasser, R. M. Unusual Vibrational Dynamics of the Acetic Acid Dimer. *J. Chem. Phys.* **2001**, *115*, 7629−7643.

(45) Prada-Gracia, D.; Shevchuk, R.; Rao, F. The Quest for Self-Consistency in Hydrogen Bond Definitions. *J. Chem. Phys.* **2013**, *139*, 084501.

(46) Robertson, E. J.; Carpenter, A. P.; Olson, C. M.; Ciszewski, R. K.; Richmond, G. L. Metal Ion Induced Adsorption and Ordering of Charged Macromolecules at the Aqueous/Hydrophobic Liquid Interface. *J. Phys. Chem. C* **2014**, *118*, 15260−15273.

(47) Johann, R.; Vollhardt, D.; Mohwald, H. Study of the pH Dependence of Head Group Bonding in Arachidic Acid Monolayers by Polarization Modulation Infrared Reflection Absorption Spectroscopy. *Colloids Surf., A* **2001**, *182*, 311−320.

(48) Muro, M.; Itoh, Y.; Hasegawa, T. A Conformation and Orientation Model of the Carboxylic Group of Fatty Acids Dependent on Chain Length in a Langmuir Monolayer Film Studied by Polarization-Modulation Infrared Reflection Absorption Spectroscopy. *J. Phys. Chem. B* **2010**, *114*, 11496−11501.

(49) Soule, M. C. K.; Blower, P. G.; Richmond, G. L. Effects of Atmospherically Important Solvated ions on Organic Acid Adsorption at the Surface of Aqueous Solutions. *J. Phys. Chem. B* **2007**, *111*, 13703−13713.

DOI: 10.1021/acs.jctc.5b00484
J. Chem. Theory Comput. 2015, 11, 4780−4790